Journal of Power Sources 196 (2011) 2433–2444

Contents lists available at ScienceDirect

Journal of Power Sources

journal homepage: www.elsevier.com/locate/jpowsour

Review

Palladium-based electrocatalysts for hydrogen oxidation and oxygen reduction reactions

Minhua Shao*

UTC Power, 195 Governor's Highway, South Windsor, CT 06074, USA

ARTICLE INFO

Article history:
Received 10 September 2010
Received in revised form 27 October 2010
Accepted 28 October 2010
Available online 3 November 2010

Keywords:
Palladium
Electrocatalysts
Fuel cells
Platinum
Oxygen reduction reaction
Hydrogen oxidation reaction

ABSTRACT

Fuel cells, especially low temperature fuel cells are clean energy devices that are expected to help address the energy and environmental problems that have become prevalent in our society. Platinum-based electrocatalysts are usually used as the electrocatalysts for both the anode (hydrogen oxidation) and cathode (oxygen reduction) reactions. The high cost and limited resources of this precious metal hinder the commercialization of fuel cells. Recent efforts have focused on the discovery of palladium-based electrocatalysts with little or no platinum for hydrogen oxidation reaction (HOR) and oxygen reduction reaction (ORR). This paper overviews the recent progress of electrocatalysis of palladium-based materials including both extended surfaces and nanostructured ones for HOR and ORR. The properties of CO and methanol tolerances of palladium-based electrocatalysts are also summarized.

Contents

1. Introduction

Fuel cells, and especially low temperature fuel cells such as proton exchange membrane fuel cells (PEMFCs), direct alcohol fuel cells (DAFCs) and alkaline fuel cells (AFCs), are clean energy devices that are expected to help address the energy and environmental problems that have become prevalent in our society. Despite their great promise, existing fuel cell technologies have some drawbacks such as efficiencies that are lower than theoretically predicted, the high Pt content of state-of-the-art electrocatalysts, and the performance decay during fuel cell operation [1,2].

In a low temperature fuel cell, hydrogen gas is oxidized into protons, electrons, and other byproducts when other fuels are used at the anode. At the cathode of the fuel cell, the oxygen is reduced, leading to formation of water. Both the anodic and cathodic reactions require electrocatalysts to reduce the overpotentials and

* Tel.: +1 860 727 7251; fax: +1 860 660 7384.
E-mail address: Minhua.shao@utcpower.com

0378-7753/$ – see front matter © 2010 Elsevier B.V. All rights reserved.
doi:10.1016/j.jpowsour.2010.10.093

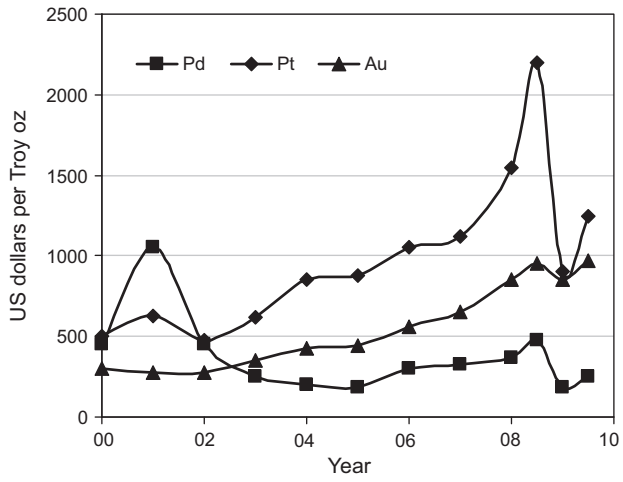

Fig. 1. Comparison of the cost of Pd, Pt and Au per troy ounce in the period of 2000–2009.
Data from Ref. [6].

increase reaction rates. Pt-based materials are usually used as the electrocatalysts for both the reactions, however, the high cost and limited resources of this precious metal are hindering the commercialization of fuel cells. Recent efforts have focused on the discovery of electrocatalysts with little or no Pt for hydrogen oxidation reaction (HOR) and oxygen reduction reaction (ORR) [3–5].

With the exception of Pt, the electrocatalytic activity of Pd is one of the highest among the pure metals for both HOR and ORR. This, combined with the fact that the cost of Pd is lower than that of Pt, makes it an attractive alternative. Fig. 1 compares the prices per troy ounce of Pd, Pt and Au in the last ten years [6]. In general, the cost of Pd is one quarter of Pt and half of Au except in the period of 2000–2002 when it spiked to $1100 per troy oz due to insufficient supply in the market. However, without a good estimation of available resources and future demands, it is difficult to project the future cost of Pd. Fig. 2 shows the demand of Pd in different industrial sectors [7]. Similar to Pt, most Pd today is used in the automotive industry for catalytic converters to reduce the toxicity of emissions from a combustion engine.

While Pd is less expensive than Pt, the electrocatalytic activities of pure Pd for HOR and ORR are at least five times lower than that of Pt, which prevents it from being used directly in fuel cells. Great efforts have been dedicated to improve the activity of Pd by surface modification and alloying. This paper attempts to summarize the recent progress of electrocatalysts containing Pd for HOR and ORR. The development of Pd electrocatalysts for electro-oxidation of small organic molecules is not discussed in this paper, but has been adequately covered in the recent reviews by Antolini [8], Bianchini and Shen [9].

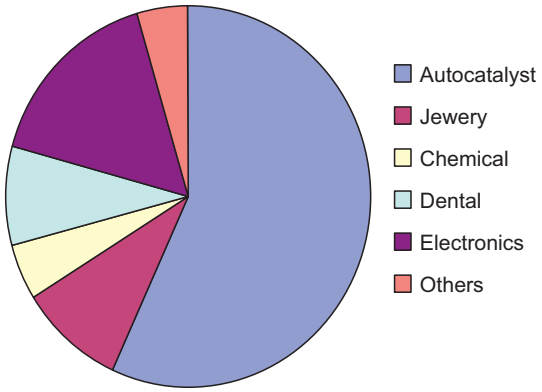

Fig. 2. World-wide demands for Pd from different industrial sectors.

2. Hydrogen oxidation reaction (HOR)

2.1. HOR on bulk surfaces

The hydrogen oxidation reaction (HOR) $H_2 \rightleftarrows 2H^+ + 2e^-$, has been extensively studied on Pt surfaces [10–15]. There are three elementary reaction steps for HOR on a Pt surface, based on the Tafel–Heyrovsky–Volmer mechanism [16–18]:

$$H_2 \rightleftarrows H_{ad} + H_{ad} \quad \text{Tafel reaction} \tag{1}$$

$$H_2 \rightleftarrows H_{ad} + H^+ + e^- \quad \text{Heyrovsky reaction} \tag{2}$$

$$H_{ad} \rightleftarrows H^+ + e^- \quad \text{Volmer reaction} \tag{3}$$

In the Tafel–Volmer reaction pathway, the dissociative adsorption of a H_2 molecule is followed by the one-electron oxidation of the adsorbed H atoms. In the Heyrovsky–Volmer reaction pathway, a one-electron oxidation occurs simultaneously with the dissociative adsorption of a H_2 molecule, followed by another one-electron oxidation of the adsorbed H atom. Recent modeling and experimental work [12–14] has demonstrated that the fast, inversed exponential rising of kinetic current at overpotential (η) less than 50 mV mainly results from the Tafel–Volmer pathway, while a much more gradual current rise at higher overpotentials corresponds to a Heyrovsky–Volmer pathway.

Since the electronic properties of Pd are very similar to Pt, the HOR on Pd surfaces may follow the same pathways proposed for Pt. However, the strong hydrogen absorption behavior of Pd bulk electrodes has prevented the practical HOR studies on such surfaces [19,20]. Very recently, Rau et al. [21] measured the HOR polarization curves, as shown in Fig. 3, on a Pd thin film supported on an Au rotating disk electrode in a H_2SO_4 solution. Two stages of HOR were observed at overpotentials lower than 100 mV. In the low overpotential region of $\eta < 40$ mV, the rapid current density originates from the oxidation of β Pd–H, a hydride with a high H content. On the other hand, the oxidation of α Pd–H, a solid solution with a low H concentration, is responsible for the current increase in the high overpotential region of $\eta > 100$ mV. The current plateau

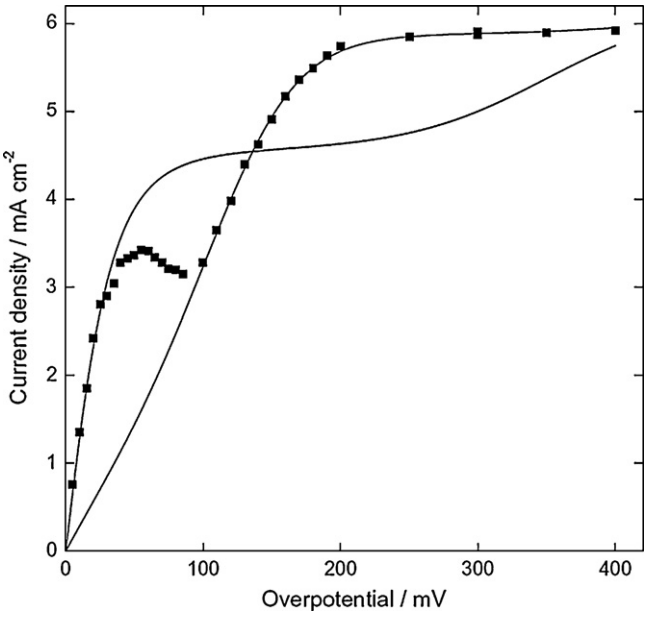

Fig. 3. Hydrogen oxidation polarization curve on a Pd film electrode recorded in 0.5 M H_2SO_4 at ω = 8100 rpm. (■) Experimental; (—) simulation [21].

in the overpotential region of 40 mV < η < 100 mV corresponds to the transition of β to α Pd–H phase. Unlike on the Pd bulk surface, hydrogen adsorption and absorption features can be distinguished on the surface of Pd nanoparticles, which may allow us to study the hydrogen oxidation kinetics of Pd by using micro-electrode technique. Recently, Chen and Kucernak [12] investigated the rapid kinetics of the HOR on a single Pt nanoparticle with a particle size of 40 nm. The high mass transport rates on such a small particle enable them to measure the kinetic current density of HOR more accurately. The HOR kinetics on Pd surface may be studied using the micro-electrode technique to further understand the HOR mechanisms.

The dissociative adsorption of H_2 on the catalyst surfaces, involving the electron transfer from the surface to the σ^* antibonding orbital of the H_2 molecule, is the rate-determining step of HOR. Consequently, the interaction of M–H_{ad} plays a dominant role in the kinetics of HOR. Following the Sabatier principle, a surface with a M–H_{ad} binding energy that is either too strong or too weak may result in a poor catalyst for HOR. Volcano-type plots have been rationalized by Parsons [22] and Gerischer [23], and later Krishtalik [24] and Trasatti [25], who found that the logarithm of the exchange current densities of hydrogen evolution reaction (HER) correlated well with the standard free energy of adsorption of hydrogen (ΔG_H), with the maximum near $\Delta G_H = 0$.

Using density functional calculations (DFT), Norskov et al. [26,27] recently calculated the hydrogen chemisorption energies, from which the ΔG_H were derived. The authors demonstrated that active HER catalysts, such as Pt with a ΔG_H near zero (−0.09 eV), bind hydrogen neither too strongly nor too weakly, and consequently all reaction steps are thermo-neutral on such catalysts at the equilibrium potential. The interaction of Pd–H_{ad} is stronger than Pt–H_{ad} as evidenced by a more negative ΔG_H for Pd than Pt. The strong adsorption of hydrogen on Pd causes a slow reaction rate of the oxidation of H_{ad} (Volmer reaction) and consequently blocks the adsorption sites for H_2 molecules, resulting in a slow overall HOR/HER reaction rate. Since the kinetics of HOR/HER strongly depends on the electronic properties of the surface, they can be enhanced by proper surface modification. Markovic et al. [28] have demonstrated that the HOR kinetics on Pt(1 1 1) could be enhanced significantly by depositing a Pd monolayer (ML) on it. The activity improvement can be interpreted by a weaker M–H_{ad} interaction on Pd/Pt(1 1 1) than on the bare Pt surface. Greeley et al. [29] correlated ΔG_H of Pd monolayer on various other noble metals/alloys with their HER activities and found a similar volcano plot (Fig. 4) with Pd/PtRu residing near the peak at $\Delta G_H = 0$. The HER on the materials on the left branch of the volcano curve is limited by the oxidation of H_{ad} (Volmer reaction) due to strong M–H_{ad} interactions. If the data of ΔG_H of Pt and Pd from the same group are included in the plot [26], it is clear that they are on the left branch of the volcano curve and Pd/Pt(1 1 1) is closer to the volcano peak than Pd(1 1 1) or Pt(1 1 1) resulting from the downshift of the *d*-band center away from the Fermi level. Thus, one may expect that the activity should follow the trend of Pd/Pt(1 1 1) > Pt(1 1 1) > Pd(1 1 1), in good agreement with Markovic's findings [28]. Generally, the activity of HOR follows the same trend of HER on noble metal surfaces due to the high reversibility of these two reactions.

Pd/Au(1 1 1) should have a lower HOR activity due to the stronger H_{ad} adsorption than on pure Pt as indicated in Fig. 4. In fact, Schmidt et al. found that Pd/Au(1 1 1) showed one order of magnitude lower activity than the Pt(1 1 1) surface [30]. However, this surface has a higher CO tolerance compared to pure Pd and Pt. The CO adsorption energy is significantly reduced on Pd/Au(1 1 1) surfaces in comparison to pure Pd based on the DFT calculations [31]. The weaker CO adsorption may be responsible for the improved capability of oxidation of CO on the Pd monolayer surface on Au. However, Ruvinsky et al. [32] recently found that the CO stripping occurred at more positive potentials on a submonolayer of Pd on Au/C than on a pure Pd/C surface, even though the former surface had a higher CO tolerance. This discrepancy can be explained by the stronger OH adsorption on Pd/Au than on bulk Pd.

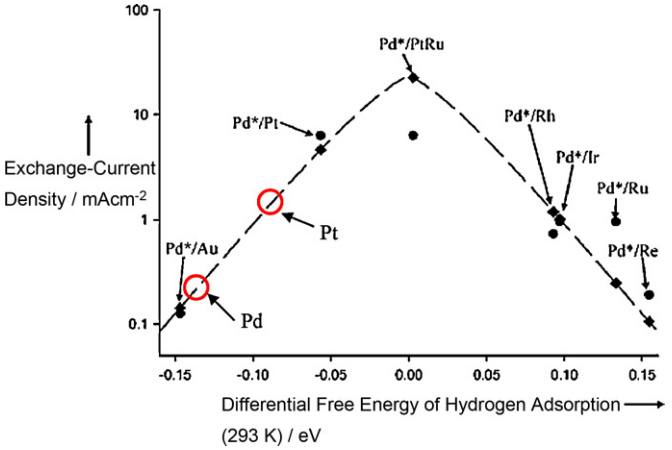

Fig. 4. Hydrogen evolution exchange current density as a function of the theoretical differential free energy of hydrogen adsorption (ΔG^*_H). The dashed line shows the functional form of the theoretical exchange-current density, as predicted by the model, and the black diamonds correspond to the predictions for specific overlayers. The black circles represent experimental measurements. Pd*/X denotes a pure overlayer of Pd on a substrate of metal X [29]. The red hollow circles represent the exchange current densities of pure Pd and Pt predicated by using the differential free energy of hydrogen adsorption data of Pd and Pt in Ref. [26]. (For interpretation of the references to color in this figure legend, the reader is referred to the web version of the article.)

2.2. HOR on Pd based nanomaterials

The Pt loading in a state-of-the-art PEM fuel cell can be reduced to as low as 0.05 mg cm^{-2} without a noticeable drop in the cell performance due to the very fast HOR kinetics on Pt surfaces [33]. While this results in a cheaper fuel cell, the extremely low Pt loading has a potential concern of being poisoned easily by contaminants in the hydrogen feed. Recent efforts focus on developing low cost and high contamination (mainly CO) tolerant anode catalysts for PEM fuel cell. In acidic solution, Pd/C and Pt/C showed comparable HOR activity in the thin-film rotating disk electrode (TF-RDE) measurements [34]. It is very difficult to establish a reliable activity trend using RDE due to the fast kinetics of HOR on Pt and Pd, and limited mass transport rate in this method. It is generally accepted that Pd/C is at least one order of magnitude less active than Pt/C according to some recent PEM fuel cell testing results [35–37]. Pronkin et al. [38] measured the HOR of Pd/C using RDE and found an exchange current density of ~0.22 mA cm^{-2}, which is two orders of magnitude lower than that of Pt/C measured by gas diffusion electrode. In our gas diffusion electrode measurement, the exchange current density of Pd/C was much higher than 0.22 mA cm^{-2} [39], suggesting that the HOR kinetics on Pd/C is still too fast to be measured by a regular RDE experiment. The exchange current densities of HOR on Pd/C and Pt/C are underestimated in RDE measurements due to low utilization and limited mass transport rate. Extra care need to be taken when one compares the actual activity numbers measured by different techniques. More suitable techniques like hydrogen pump [40], micro-electrode [12], gas diffusion electrode [41], and rotating disk electrode with ultralow catalyst loading [42] are needed to measure the HOR activities for Pd based electrocatalysts.

By changing the H_{ad} binding energy, it is possible to increase the HOR rate on the catalytic surfaces as discussed. Binary Pd–Pt based anode catalysts have caught significant attention since Stone-

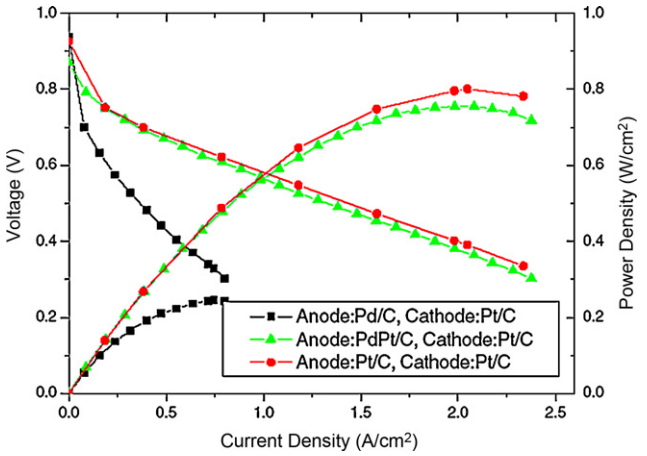

Fig. 5. Comparison of single cell performance fabricated with electrodes of Pt/C, Pd/C and PdPt/C as anode, respectively. All the cathode electrodes were made with Pt/C [37].

hart observed a comparable performance to Pt/C in the phosphoric acid fuel cells (PAFCs) by alloying Pd with Pt [43,44]. The similar high HOR activity has been confirmed in PEM fuel cells. Cho et al. [37] found that there was no noticeable difference in performance whether Pt/C or $Pd_{19}Pt/C$ was used as the anode catalyst as shown in Fig. 5. The comparable HOR activities of Pd–Pt alloys with Pt have also been observed by other groups [35,36,45,46]. It was suggested that a Pd enriched skin layer, which was formed in the Pd–Pt alloys, was responsible for the enhanced HOR activity [47]. Similar to the system of Pd/Pt(1 1 1), the Pd–H_{ad} binding strength on the Pd skin layer is lower than that on a bulk Pd surface. However, no solid evidence is available suggesting the formation of Pd-enriched surface. Yoo et al. [48] studied the HOR activity on PdPt alloys with various Pd:Pt ratios. They found that the exchange current densities of PdPt alloys followed a volcano trend, with $Pd_{30}Pt_{70}$ being the most active. After charging with hydrogen, the density of states (DOS) of Pt was significantly modified by the Pd-absorbed hydrogen. DFT calculations revealed that the *d*-band center of Pt was downshifted in ambient air but it was upshifted due to the formation of Pd hydride. The upshifting of the *d*-band center of Pt was confirmed by the increase of its *d*-band vacancies measured by the X-ray absorption spectroscopy. The maximum activity observed on $Pd_{30}Pt_{70}$ was explained by the stronger Pt–H_{ad} binding energy than pure Pt. The HOR activities dropped with further increasing the Pt–H_{ad} strength (Pt *d*-band vacancies). However, it is not clear why a stronger Pt–H_{ad} interaction results a higher HOR activity since a lower activity would be expected according to Fig. 4.

Whether the HOR activities of Pd–Pt/C alloys are higher than or comparable to Pt/C is still under debate. Different HOR activities with respect to Pt/C were observed for Pd_xPt/C. The discrepancy may come from the variations in catalyst synthesis (particle size, alloy degree, distribution, etc.) and the electrode preparation in fuel cell testing. One may also keep in mind that the direct comparison of fuel cell performance with high noble metal loading in anode may not be appropriate. As seen in the work performed at General Motors, the Pt loading can be reduced from 0.4 to 0.05 mg cm^{-2} without sacrificing performance [33]. One may notice that the Pd–Pt loadings at the anode in the fuel cell reported in the literatures are much higher than 0.05 mg cm^{-2} resulting in a low utilization of the catalysts [37,45,46]. It is unclear whether Pd–Pt/C can maintain similar performance upon significant loading reduction of noble metal. The direct comparison of fuel cell performance with different anode materials should be made with low noble metal loadings, for instance, 0.05 mg cm^{-2}, to avoid uncertainty caused by low utilization of the catalysts.

2.3. CO tolerance on Pd based nanomaterials

Pd alloys (mainly Pd–Au and Pd–Pt) were found to be superior to Pt as the anode catalyst in PAFCs due to their higher CO tolerance [44,49,50]. It is known that the rate determining step (Tafel step) of HOR on Pt and Pd surfaces needs two adjacent Pt sites for H_2 adsorption and dissociation. Similar to Pt, pure Pd does not have good tolerance because the M–CO (M = Pd, Pt) bond is stronger than M–H causing a dramatic decrease of free sites available for H_2 dissociation even with only a trace of CO in the fuel. Two strategies may be considered to design anode electrocatalysts with high CO tolerance. One is to accelerate the CO oxidation by providing active OH_{ad} at much lower potentials. A typical system is PtRu electrocatalyst, in which Pt–CO_{ad} reacts with Ru–OH_{ad} at low potentials releasing more Pt sites for H_2 oxidation. The other way is to weaken the strength of CO adsorption on the catalyst surface. The Pd-based alloys are synthesized based on this strategy. At room temperature, both Pt/C and Pd–Pt/C surfaces are fully blocked by CO. At 80 °C, the Pt/C surface was fully covered by CO, while the CO coverage decreased on Pd–Pt alloy surfaces with increasing Pd content [51]. This result suggests that the CO binding on Pd–Pt alloy surfaces is weaker than on pure Pt or Pd surfaces. The PEMFC testing results revealed that the inclusion of Pd in the anode electrocatalysts, such as Pt and PtRu, leads to enhanced CO tolerance of these catalysts [47,51]. For the Pd–Pt/C catalysts fueled with H_2/CO, there was no CO_2 emission at the PEMFC anode outlet, indicating that the improved CO tolerance is due to the weaker CO adsorption on the alloy surfaces compared to that on pure Pd or Pt [47]. Pd–Au/C nanoparticles also showed superior CO tolerance than pure Pd/C, Pt/C and even PtRu/C [34,52,53]. The enhanced CO tolerance was proposed to originate from the much weaker CO adsorption energy and consequently more active Pd sites for H_2 oxidation on Pd–Au surfaces in comparison to other systems [52]. The high CO tolerance may also be due to the high CO oxidation activity of small Au clusters in the Pd–Au system [54].

Pd-based electrocatalysts have been demonstrated to be promising candidates to replace pure Pt/C as anode materials for PEMFC owing to their lower cost, higher activity (some of them) and better CO tolerance. However, there is also concern about the stability of such nanoparticles in a H_2 environment due to structural disorder in the alloys caused by the strong absorption of H_2 [55]. When the Pd nanoparticle is fully charged with H_2, the lattice constant increases and the volume of the particle expends by ~10%. The Pd structure returns to normal once the H_2 is discharged from the Pd lattice. There is no information available regarding the stability of Pd atoms during the lattice expansion and charge–discharge cycle of H_2. Long-term stability testing of Pd-based materials in a H_2 environment is needed to address such questions.

3. Oxygen reduction reaction (ORR)

3.1. ORR on bulk surfaces in acidic solutions

The study of ORR on Pd bulk electrodes in acidic media has received less attention than on Pt due to the lower activity and stability of the former. Damjanovic and Brusic [56] found that the exchange current densities for a polycrystalline Pd and Pt electrode are 2×10^{-11} and 10^{-10} A cm^{-2}, respectively in $HClO_4$ solution. It has been well known that the ORR kinetics strongly depends on the crystallographic orientation of the electrodes and on the electrolyte used in the experiment. For instance, in H_2SO_4 solutions, the ORR activity of low index planes of Pt follows the order of Pt(1 1 1) < Pt(1 1 0) < Pt(1 0 0), while in the $HClO_4$ solutions, it follows the order of Pt(1 0 0) < Pt(1 1 1) ≤ Pt(1 1 0) [57]. The main reason for the lower activity of Pt(1 1 1) than Pt(1 0 0) in H_2SO_4

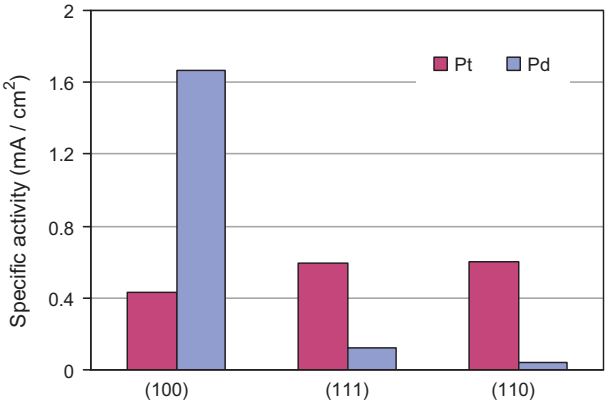

Fig. 6. Comparison of specific activity of oxygen reduction on low index facets of Pd and Pt single crystals at 0.9 V.
Data from Ref. [58].

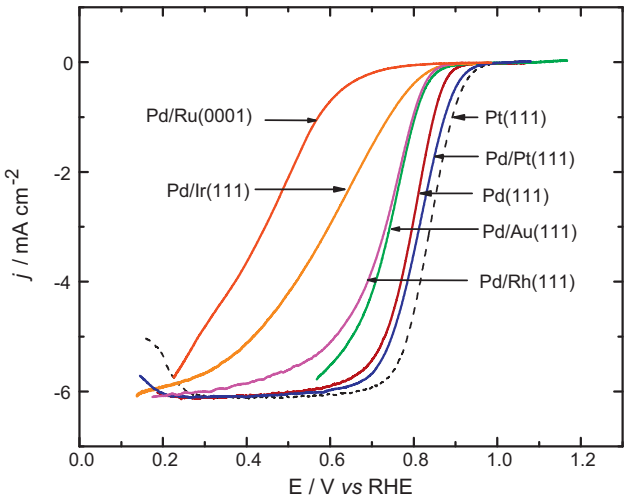

Fig. 7. Comparison of polarization curves for ORR on Pd(1 1 1), Pt(1 1 1) and Pd monolayers on different substrates in 0.1 M $HClO_4$ solution; sweep rate 10 mV s^{-1}; room temperature [68].

solutions is the much stronger adsorption of SO_4^{2-} and HSO_4^- on the former. On the other hand, there is no anion strongly adsorbed on either surface in the $HClO_4$ solutions. In such electrolytes, the discrepancy of the activity on the different surfaces originates primarily from the structural and electronic properties of the surfaces rather than from the poisoning effect from specific adsorption of the anions.

Not until very recently have the facet dependent ORR activities of the Pd single crystals been available. Kondo et al. [58] measured the ORR activities of low index planes of Pd single crystals in $HClO_4$ solution with a rotating disk electrode and found that the activity increased following the order of: Pd(1 1 0) < Pd(1 1 1) ≪ Pd(1 0 0). This order is completely opposite to that on Pt in the same solution. The comparison of the kinetic activities on different Pd and Pt facets is shown in Fig. 6. Surprisingly, the activity of Pd(1 0 0) is 14 times and nearly 3 times as high as that of Pd(1 1 1) and Pt(1 1 1), respectively. The kinetic current densities of ORR correlate well with the terrace atom density on n(1 0 0)–(1 1 1) and n(1 0 0)–(1 1 0) series of Pd suggesting that (1 0 0) atoms are the most active sites for ORR on Pd electrodes. Further fundamental studies are needed to understand the mechanisms of facet dependence of ORR activity on Pd(h k l). If these results are true, they will be important to guide the design of more active Pd based catalysts, which may consist of a large fraction of (1 0 0) facets.

In acidic media, Pd has a higher ORR activity than any other noble metals, except for Pt. The ORR mechanisms on Pt surfaces are not fully understood despite the extensive studies conducted during the past five decades [59–61]. It is generally accepted that the first electron transfer or oxygen adsorption together with an electron and proton transfer forming superoxide is the rate-determining step on a Pt surface. A more reactive surface with a higher d-band center, tends to bond the adsorbates more strongly, and consequently the electron transfer and O–O bond breaking are much easier [56]. However, the kinetics of the consequent reduction/hydrogenation of the adsorbates (O, OH) may be slow due to the strong adsorption of these species. Thus, a good ORR catalyst is one that forms a moderate bond with the adsorbates to balance the kinetics of O–O bond breaking and removal of oxygen-containing species generated from the former step. Mavrikakis et al. [62] and Norskov et al. [63] found that the oxygen binding energy (BEo) on Pt(1 1 1) is a little bit too strong. If slightly weakened, such as found for a surface of Pt/Pd(1 1 1) [64] and for a Pt skin on various Pt alloys [63,65,66], the ORR activity can be enhanced remarkably. Pd is a relatively reactive metal. It oxidizes at more negative potentials than Pt; thus, its position is on the ascending branch of the volcano plot for the ORR below Pt [67].

One way to improve the ORR kinetics of Pd surfaces is to reduce the BEo by lowering its d-band center. The DFT calculations reported by Shao et al. [68] revealed that the Pd monolayer on Pt(1 1 1) has a lower d-band center than a bare Pd(1 1 1) surface and hence a lower BEo, making Pd/Pt(1 1 1) a better catalyst than Pd(1 1 1) for ORR. This argument was supported by their experimental work, which showed that Pd/Pt(1 1 1) had a higher ORR activity than Pd(1 1 1), but somewhat lower than Pt(1 1 1) as shown in Fig. 7 [68].

Pd is more sensitive to anion adsorption than Pt due to the stronger interaction between the Pd surface and anions (Cl^-, ClO_4^-, SO_4^{2-}, and other oxygen-containing species). Climent et al. [69], Arenz et al. [70] and Shao et al. [68] studied the Pd ML-modified Pt(1 1 1) (Pd/Pt(1 1 1)) surface and found that it was less active for ORR than bare Pt(1 1 1) in a $HClO_4$ solution due to the enhanced anion adsorption. The binding energies of not only oxygen reduction intermediates, but also other anions such as Cl^-, SO_4^{2-}, HSO_4^-, and ClO_4^-, are stronger on Pd than on Pt surfaces. The strongly adsorbed anions on Pd occupy the sites for O_2 adsorption and O–O bond breaking, resulting in a slower ORR reaction rate than Pt in all the acidic media investigated so far. As shown in Fig. 8 [70], 10^{-6} M Cl^- in a $HClO_4$ solution does not affect the 4-electron reduction pathway on Pt(1 1 1) with negligible H_2O_2 produced before the potential reaches the H_{upd} region, though it is noted that the adsorbed Cl^- does inhibit the ORR in the low overpotential region. On the other hand, the strong adsorption of Cl^- on Pd/Pt(1 1 1) makes the surface much less active for ORR with significantly higher H_2O_2 production than in the solution without Cl^- at all potentials. The high yield of H_2O_2 corresponds to a 3.5-electron reduction pathway in the potential range of 0.3 V < E < 0.7 V. These results imply that even with a tiny contamination in the solution, the ORR activity measurements of Pd-based electrocatalysts in the liquid cell can be underestimated remarkably.

3.2. ORR on bulk surfaces in alkaline solutions

Lima et al. studied the ORR activities of different noble metals with a (1 1 1) facet in a 0.1 M NaOH solution [71]. The results showed that Pd(1 1 1) was more active in an alkaline solution than in an acidic solution, with an ORR activity very close to that of Pt(1 1 1) in the former solution. A similar volcano-type of activity and d-band center relationship as discussed in the acidic solution were observed and are shown in Fig. 9. In alkaline solutions,

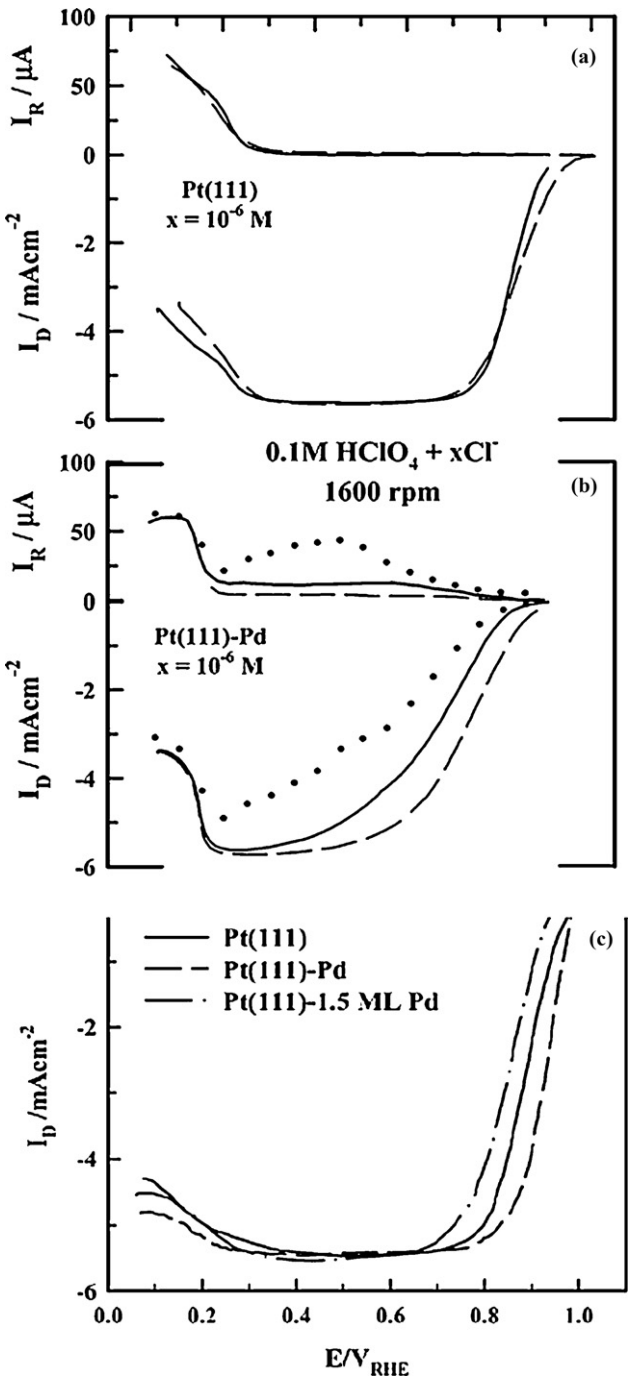

Fig. 8. Polarization curves for the ORR and corresponding peroxide oxidation current on the ring electrode in 0.1 M $HClO_4$ containing different amounts of chloride; 50 mV s^{-1}, 293 K. Dashed line, no chloride added; full line, 10^{-6} M added for (a) Pt(1 1 1) and (b) Pd monolayer on Pt(1 1 1), respectively; thick dots represent steady-state currents after 1 min coming from the negative potential limit. (c) Polarization curves for the ORR on Pd overlayer on Pt(1 1 1) disk electrodes in 0.1 M KOH; 50 mV s^{-1}; 293 K [70].

Pd(1 1 1) is more close to the top of the volcano than in acidic solutions.

Arenz et al. found that Pd/Pt(1 1 1) has a higher ORR activity than Pt(1 1 1) in alkaline solution, which is different than in acid solution [70]. In alkaline solution, where only OH anions are present, the inhibition effect from the strong anion adsorption is much smaller than in acidic solution, resulting in a high ORR activity. Pd overlayers on Au(1 0 0) and Au(1 1 1) also showed significant activity improvement with respect to an unmodified Au substrate in the

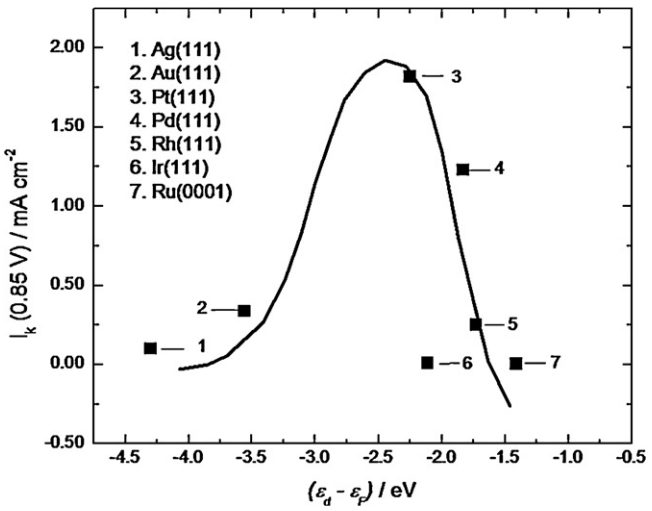

Fig. 9. Kinetic currents at 0.80 V for oxygen reduction on the different metal single crystals in 0.1 M NaOH solution as a function of the calculated metal *d*-band center relative to the Fermi level [71].

alkaline solutions [72–74]. The very high activity of Pd in alkaline solutions is surprising and deserves further attention.

3.3. ORR on Pd-based nanocatalysts

More active and durable ORR electrocatalysts have been developed for PAFC by alloying Pt with transition metals M (M = V, Cr, Co, Ni, Fe, Ti, etc.), with control of their properties being achieved by adjusting the Pt:M ratios and annealing temperatures [75–77]. Similar activity improvement from Pt alloys has been observed in PEMFC operated in relatively lower temperatures than PAFC. The activity enhancement mechanisms have been an open question for three decades and ascribed to decreased Pt–Pt bond distance [78], enhanced surface roughness [79], increased Pt *d*-band vacancy [80–82], weakened OH adsorption [83,84], and downshifted *d*-band center [62,85–89]. Recently, Nørskov et al. and Mavrikakis et al. combined the structural and electronic effects by introducing a *d*-band model that correlates changes in the energy center of the valence *d*-band density of states at the surface sites with their ability to form chemisorption bonds. According to their model, the binding energy of oxygen containing species on Pt skin formed during selective leaching of non-noble metals or annealing at high temperatures were weaker than on a pure Pt surface due to the compressive strain and electron transfer from the transition metal on the subsurface layer. Similar to Pt, the activity of Pd can be enhanced by alloying with transition metals.

3.3.1. ORR in acidic solutions

The ORR activity of Pd/C is generally five times lower than that of Pt/C in perchlorate acid due to the stronger binding energy of oxygen containing species on the surface of the former [90]. This ratio is similar to that observed on extended surfaces [56,91]. Savadogo et al. [92] for the first time observed the enhanced ORR activities on sputtered Pd–Co, Ni, and Cr bulk alloys in acidic solutions. Since their pioneering work, many groups have reported the oxygen reduction behaviors of Pd based nanoparticles.

Using scanning electrochemical microscopy (SECM) as a screening technique, Bard's group [93–95] identified a series of Pd-based catalysts, including binary systems Pd–Co, Mn, V, Ti, and ternary systems Pd–Co–Au [93,94], Pd–Co–Mn [96], that showed higher ORR activity than pure Pd. Some of the catalyst combinations exhibited ORR activities comparable to or even higher than that of Pt/C in fuel cell testing. For Pd–Co/C, the maximum activity was observed

with a Co atomic ratio in the range of 10–20% but the high activity was lost quickly during electrochemical testing [94]. Incorporation of a third element such as Au or Mn in Pd–Co/C alloys to form a ternary system was believed to improve the stability of the catalysts without sacrificing the activity [93,96]. Indeed, Raghuveer et al. [96] found that Pd–Co–Mo catalysts with a Pd:Co:Mo atomic ratio of 70:20:10 exhibited higher activity than Pt/C, but with excellent chemical stability. Despite these promising results, one may find that the activity of the baseline Pt/C was lower than that typically reported in the literature. Mathiyarasu and Phani [97] investigated ORR activity of ternary Pd–Co–M (M = Pt, Au, Ag) catalysts. As expected, the Pd–Co–Pt combination showed the highest activity which was higher than Pt/C, but Pd–Co and Pd–Co–Au exhibited very low activity, which is contrast to other reports [68,93].

Depending on the synthesis methods and annealing temperatures, different optimum Pd:M ratios for ORR were reported. Shao et al. [68] found that Pd_2Co/C synthesized by the impregnation method and annealed at 900 °C exhibited the highest ORR activity. The same optimum ratio was also observed by Wang et al. [98], who co-reduced Pd and Co salts in ethylene glycol and annealed the dried product at 500 °C. The highest ORR activity for Pd–Co catalysts (30–40 at% Co) formed by co-reducing Pd and Co salts in aqueous solutions, was obtained by Zhang et al. [99]. Particle size, as well as the activity, increased with increasing annealing temperature, and the highest activity was observed at the lowest annealing temperature (300 °C). For the Pd–Fe systems, an optimized composition of Pd:Fe = 3:1 was found by several groups [7,90,100,101]. The ORR activity of Pd_3Fe/C was comparable to or higher than that of Pt/C. A comparison between Pd_3Fe/C and Pd_2Co/C in Fig. 10a reveals that the former has a slightly higher ORR activity [90]. A good parallelism between specific activity and the Pd–Pd interatomic distance expressed as a function of Fe content was found (Fig. 10b) [90,102]. The highest ORR activity was obtained for Pd_3Fe, which has a Pd–Pd bond distance of 0.273 nm, smaller than that of Pd by 2.3%. Similar results were obtained for the Pd–Co alloys [98], suggesting the compressed lattice constant plays a role in the activity enhancement. The activity of Pd_3Fe was found to be further enhanced by adding a small amount of Ir in it [100]. The enhancement mechanism is unknown. For Pd–W alloys annealed at 800 °C, only 5% W is needed to maximize the activity [103].

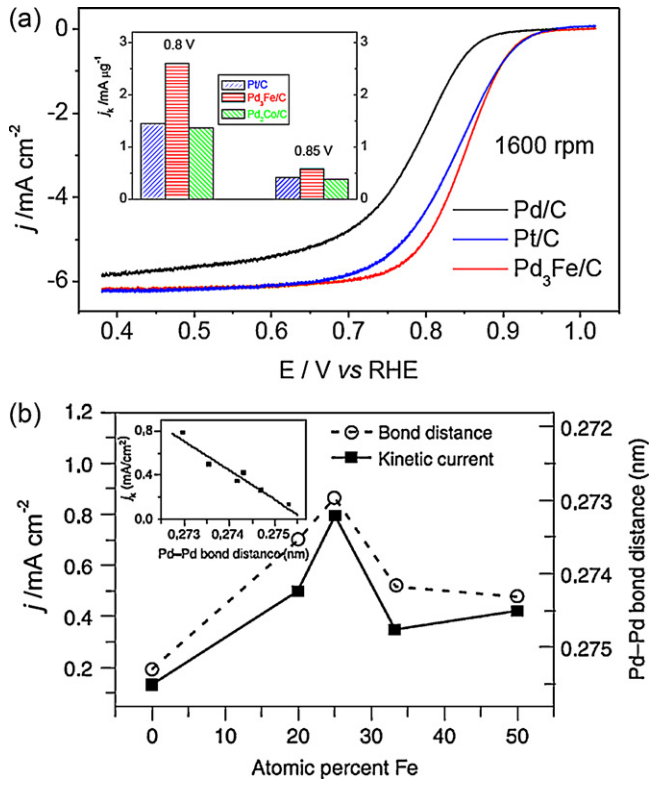

Fig. 10. (a) Comparison of polarization curves for the ORR on Pd/C (ETEK), Pt/C (ETEK) and Pd_3Fe/C nanoparticles in 0.1 M $HClO_4$. Sweep rate 10 mV s^{-1}; room temperature. The noble metal loading was controlled at 10 μg cm^{-2}. Insert: comparison of noble metal mass activity for Pt/C (ETEK), Pd_3Fe/C and Pd_2Co/C at 0.8 V and 0.85 V. (b) Specific activity and Pd–Pd bond distance calculated from XRD data against the concentration of Fe in Pd–Fe/C electrocatalysts. All samples were treated at 500 °C [90].

Oxygen reduction activities of some Pd-nonmetallic element alloys (Pd–Se, S and P) were also studied, but no significant improvements have been observed [104,105]. Further work of this type of alloys should be stopped. Pd–Pt alloys, however, showed higher ORR activity than Pt with a small amount of Pd in the alloys. For instance, Li et al. found that Pt–Pd/C exhibited a slightly higher ORR activity than Pt/C [106]. Guerin et al. found that the Pd–Pt alloys showed higher activity than Pt in a composition range of 70–90% Pt [107]. The high activity was also observed on dendrimer-encapsulated Pd–Pt nanoparticles containing 180 atoms with a Pt:Pd ratio of 5:1 [108]. The enhanced activity may be explained by a shorter Pt–Pt bond distance.

The activity discrepancy for Pd-based catalysts with similar compositions has been seen in the literature. One of the main reasons is that the properties of the Pd alloys highly depend on the synthesis method and post-treatment. A good example is the Pd–Cu system. Wang et al. [109,110] found that $PdCu_3$ catalysts synthesized by a colloidal method showed a higher activity than those made by thermo-decomposition, benefiting from the more uniform alloying and much smaller particle size in the former method. Raghuveer et al. [111] also concluded that the activity of Pd–Co–Au synthesized by the microemulsion method was higher than that prepared by the conventional sodium borohydride reduction method due to the smaller particle size and higher degree of alloying.

The effects of particle size and degree of alloying were studied by Liu and Manthiram in the $Pd_{70}Co_{30}/C$ catalysts [112]. Upon increasing the annealing temperature from 350 to 500 °C, the catalytic activity decreased due to increasing the alloying degree and particle size. Further increasing the annealing temperature resulted in further activity decreases, though this was attributed solely to the increase in particle size. An interesting trend is that the activity of PdCo alloy decreased with increasing the degree of alloying in the case of the same particle size. It seems that high Co content is not necessary for activity improvement. Further studies are needed to understand the role of alloying degree and transition metal contents by controlling the particle size and compositions. Due to the high surface energy of Pd, it is very difficult to synthesize monodispersed Pd–M (M = transition metals) nanoparticles with small particle size. Such studies require novel synthesis method of Pd alloys.

The ORR activity of Pd-based catalysts depends on the shape and morphology of the materials. Pd(1 0 0) exhibited the highest ORR activity among the low index facets [58]. Several studies reported the shape-dependent ORR activities in nanoscale materials. The specific activity of Pd nanorods prepared by Xiao et al. [113] was 10 times higher than that of Pd nanoparticles and comparable to that of bulk Pt as shown in Fig. 11a. The authors attributed the high activity to the contribution from (1 1 0) sites according to their DFT calculations, which is in contrast to what was observed in the single crystal work [58]. Li and Haldar [114] synthesized PdFe nanorods with a diameter of 3 nm and length of 10–50 nm, which can be controlled by the amount and type of surfactants. The PdFe nanorods demonstrated a higher PEMFC performance than commercial Pt/C in the practical working voltage region (0.80–0.65 V) as shown in Fig. 11b. Due to the higher stability and activity of nanorods in com-

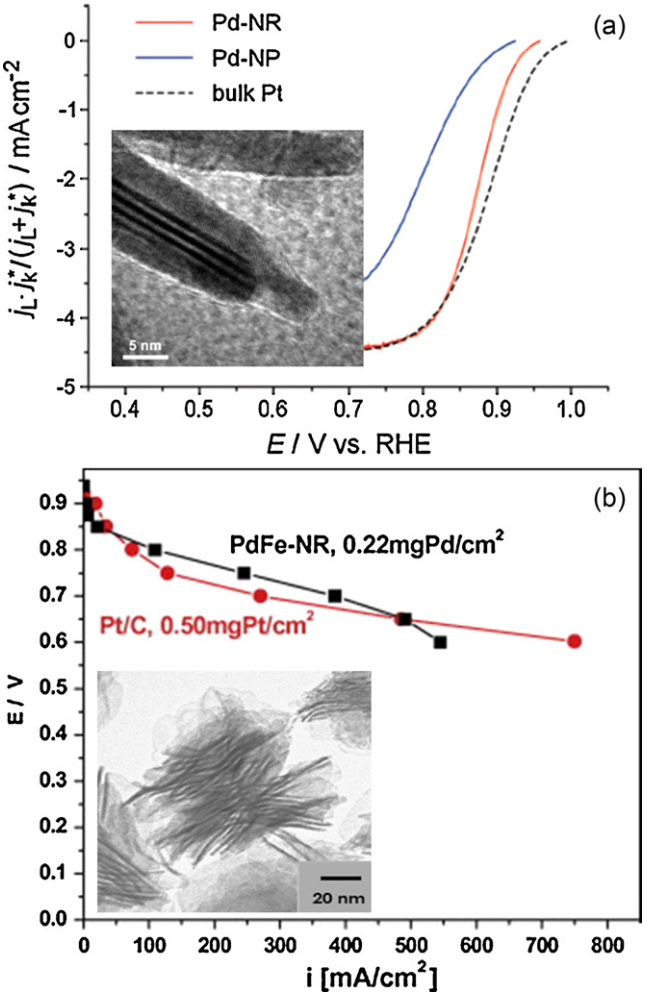

Fig. 11. (a) ORR data for Pd nanorods, Pd nanoparticle, and bulk Pt, obtained in an O_2 saturated 0.1 M $HClO_4$ solution at a rotation rate of 900 rpm and a scanning rate of 10 mV s^{-1}. The diffusion limited current has been normalized to the geometric surface area, while the kinetic current density (j_k^*) has been normalized to an electrochemical surface area. The insert is a TEM image of a Pd nanorods [113]. (b) Polarization curves of single PEMFCs with PdFe nanorods and Pt/C (BASF-fuel cell) cathode catalysts. The insert is a TEM image of unsupported PdFe nanorods [114].

parison to small nanoparticles, they could be next generation of Pd-based catalysts widely studied. The electrocatalytic activities of other shape controlled Pd-based nanomaterials (cubes, octahedra, nanowires, etc.) are also of interest.

3.3.2. ORR in alkaline solutions

Pd exhibits a higher ORR activity in alkaline than in acidic solutions due to a decrease in the anion poisoning effect in alkaline solutions. Indeed, many studies have shown that the ORR activity of Pd/C in alkaline solutions is comparable to that of Pt/C [115,116]. Similar to that of Pt/C, the ORR activity of Pd/C is dependent on the particle size of the metal. As shown in Fig. 12, Jiang et al. [116] demonstrated that the specific activity increased monotonically by a factor of about 3 with the particle size increasing from 3 to 16.7 nm, while the mass activity first increased when the Pd particle size increased from 3 to 5 nm and then decreased with further Pd particle size increases. The increase of the specific activity is contributed to the increase of the fraction of the facet atoms with increasing the particle size.

The ORR activities of Pd–M alloys (M = Fe, Ni, Au, Sn) [115,117–119] have also been studied in alkaline solutions. The Pd_3Fe/C was 2-fold more active than pure Pd/C [115]. Similar activ-

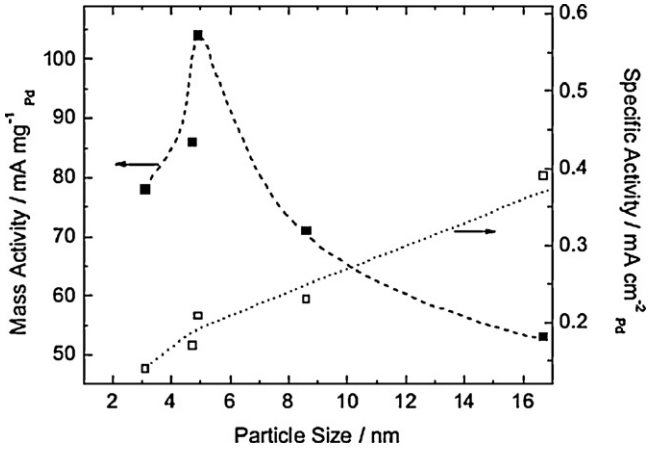

Fig. 12. Dependence of the mass activity (dashed line) and specific activity (dotted line) for the ORR on Pd/C catalysts with different Pd particle sizes in 0.1 M NaOH solution. The currents are taken at a potential of 0 V vs Hg/HgO/OH^- [116].

ity enhancement was also observed on Pd–Sn alloys [117]. For Pd–Ni/C catalyst, the ORR activity depends on the composition of the alloys. The highest activity was observed on PdNi/C and Pd_3Ni/C, which was not superior to Pd/C or Pt/C [118]. A synergistic effect from WC on ORR activity has been observed by Nie et al. [119]. The Pd nanoparticles supported on WC/C synthesized by an intermittent microwave heating method showed an enhanced ORR activity in comparison to Pd/C and Pt/C. By alloying with Au, the activity of Pd was significantly enhanced, but the exact enhancement mechanism is not clear. The strong interaction between the supports and metal nanoparticles and its effect on ORR activity may be an interesting topic to study. The development of Pd based ORR catalysts for alkaline fuel cells is of interest to replace costly Pt materials. The ORR activity and stability of Pd based catalysts, however, has to be compared to that of less expensive non-precious metal electrocatalysts [120,121]. No such study has been carried so far.

3.4. Methanol tolerance

The efficiency of direct alcohol fuel cells (DAFCs) decreases dramatically when methanol or ethanol permeates the proton exchange membrane to the cathode since the currently used Pt-containing cathode catalysts have no or little methanol tolerance. One of the advantages of Pd–M alloys over Pt in DAFCs is their high methanol and ethanol tolerance in acid. In particular, methanol tolerance was demonstrated for Pd–Fe, Pd–Co, Pd–Cr, Pd–Ni and Pd–Pt alloys [68,96,99,122–125].

Shao et al. found no evidence of methanol oxidation on Pd_2Co/C in nitrogen-saturated $HClO_4$ solution containing 0.1 M methanol (Fig. 13a) [68]. For the ORR, the half-wave potential drops *ca.* 20 mV with 0.1 M methanol in solution, compared to the same electrocatalyst without methanol. The loss of 20 mV might reflect the blocking of some active sites for oxygen reduction by the adsorbed methanol or its intermediates from oxidation. A somewhat higher methanol oxidation activity was observed by the same research group on a Pd_3Fe/C catalyst in the same electrolyte, as several small oxidation current peaks corresponding to methanol oxidation appeared (Fig. 13b). The presence of 0.1 M methanol caused a negative shift of only 10 mV in its half-wave potential despite its slightly high methanol oxidation activity. Similar methanol tolerance properties of Pd–M alloys have been reported by numerous groups [99,122,125–127]. All the results confirmed the excellent methanol tolerance of Pd-based alloys due to the low methanol oxidation on these electrocatalysts. By alloying with Pd, the methanol tolerance of Pt-based catalysts can be improved by diluting the Pt–Pt bonds,

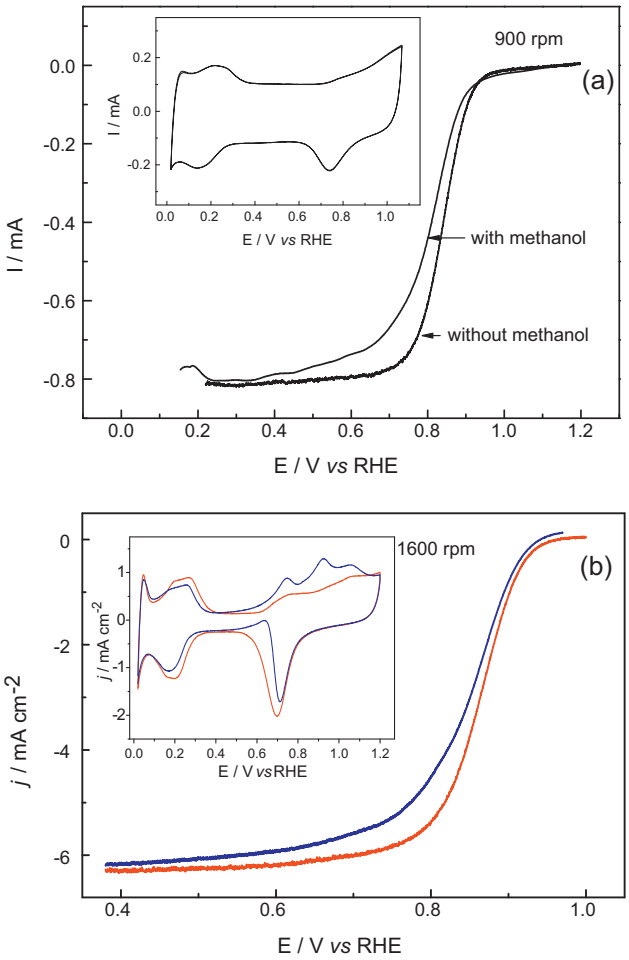

Fig. 13. (a) Comparison of polarization curves for ORR on Pd_2Co/C in oxygen saturated 0.1 M $HClO_4$ solution with and without 0.1 M methanol; rotation rate 900 rpm; sweep rate 10 mV s^{-1}. The insert is the cyclic voltammetry of Pd_2Co/C nanoparticles in nitrogen saturated 0.1 M $HClO_4$ + 0.1 M methanol solutions; sweep rates 20 mV s^{-1} [68]. (b) Comparison of polarization curves for the ORR on Pd_3Fe/C nanoparticles in 0.1 M $HClO_4$ with (blue line) and without (red line) 0.1 M methanol. Sweep rate 10 mV s^{-1}; room temperature; Pd loading 18 μg cm^{-2}. The insert is the cyclic voltammetries of Pd_3Fe/C in nitrogen saturated 0.1 M $HClO_4$ solution with (blue line) and without (red line) 0.1 M methanol. (For interpretation of the references to color in this figure legend, the reader is referred to the web version of the article.)

which are required for dissociative adsorption of methanol and ethanol on the surface of the catalyst. Accordingly, both Pd–M and Pd–Pt catalysts might be good candidates for resolving the problem of methanol crossover in DMFCs.

3.5. Mechanism of ORR activity enhancement

An understanding of the origin of the high activities of Pd–M alloys may help us in designing inexpensive and more active catalysts. Theoretical calculations and experimental data demonstrated that, upon annealing at elevated temperatures, the Pd–M alloys, like the Pt–M alloys, undergo Pd segregation, in which Pd atoms migrate to the surface to form a pure Pd skin on the bulk alloys [128–130]. The Pd lattice also contracts upon alloying with a 3d metal, which generates compressive strain in the Pd skin.

DFT calculations show that, like the Pt_3Co alloy surfaces, the electronic structure of the Pd skin is modified by strain and the underlying alloy, which in turn modifies the reactivity of the surface [131,132]. As shown in Fig. 14, compressive strain alone accounts for a 0.1 eV destabilization of the Pd–O bond. A Pd_3Fe(1 1 1) substrate contributes a further destabilization of O by *ca.* 0.25 eV,

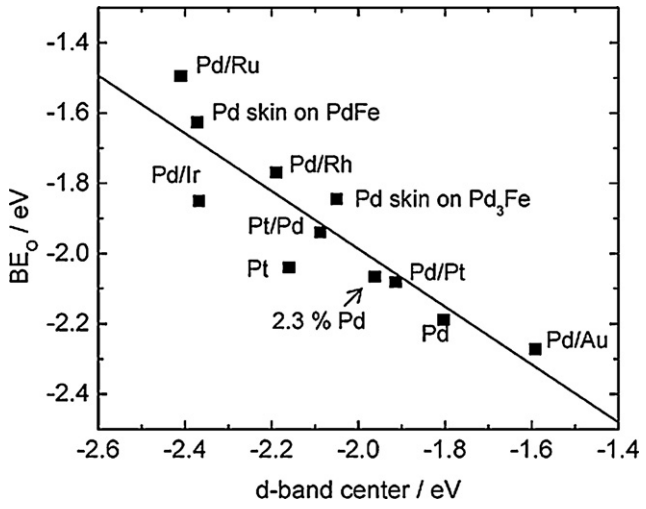

Fig. 14. Calculated oxygen-binding energies on Pd- and Pt-overlayers on various substrates as a function of the Pd *d*-band center (relative to the Fermi level). The energies plotted correspond to the most stable configuration for O adsorption at the Pd or Pt hollow sites on each surface [132].

whereas a PdFe(1 1 1) substrate contributes a further destabilization of O by *ca.* 0.35 eV. The native Pd_3Fe(1 1 1) and PdFe(1 1 1) surfaces bind oxygen *ca.* 1 eV more strongly than Pd and are therefore not expected to be good ORR catalysts. Of these surfaces, Pd skin on Pd_3Fe(1 1 1) is most similar to Pt(1 1 1) in terms of both the *d*-band center position and the oxygen binding energy, which corroborates the findings in Fig. 10b. Zhou et al. [133] recently confirmed the high activity of this alloy by using a Pd_3Fe(1 1 1) single crystal. The specific activity of an well-prepared and annealed Pd_3Fe(1 1 1) was found to be comparable to that of Pt(1 1 1). The Pt-based alloy single crystals have been extensively studied and the difference in ORR activity among pure Pt skin, skeleton and Pt–M surfaces was identified [63,66,134]. The systematic study of Pd based alloy single crystals on oxygen reduction has not been reported.

Some thermodynamic guidelines were recently proposed for designing non-Pt alloy ORR electrocatalysts. Bard and co-workers [94,95] suggested that for Pd–M alloys the reactive metal M constitutes the site for breaking the O–O bonds, forming O_{ads} that would migrate to the hollow sites dominated by Pd atoms, where it would be readily reduced to water, as shown in Fig. 15. Based on this mechanism, the alloy surface should consist of a relatively reactive metal such as Co, and the atomic ratio of this metal should be 10–20% so that there are sufficient sites for reactions of O–O bond breaking on M and O_{ads} reduction at hollow sites formed by Pd atoms. The DFT calculations [95] indicated that one of the O atoms diffused to the Pd hollow site while the other still adsorbed on the hollow site near Co after the dissociative adsorption of the O_2 molecule. The second O_2 could dissociate on Co with an O atom pre-bound on the hollow site near it. Balbuena and Wang [135], and Savadogo et al. [136] proposed a similar thermodynamic guideline for designing Pd alloy catalysts. For Pd with fully occupied valence *d*-orbitals, alloying with transition metals, such as Co with unoccupied valence *d*-orbitals, significantly reduces the Gibbs free energy both for the first charge-transfer step, and for the steps involving the reduction of intermediates. However, it is not clear whether O_2 can still easily dissociate after the reactive metal centers are fully occupied by O. Also, the reactive metals on the alloy surface are unstable and form oxides easily during the catalyst preparation process and exposing to the air, and leach out rapidly during electrochemical measurements. Thus, the effect from transition metals in the top layer on ORR may be negligible.

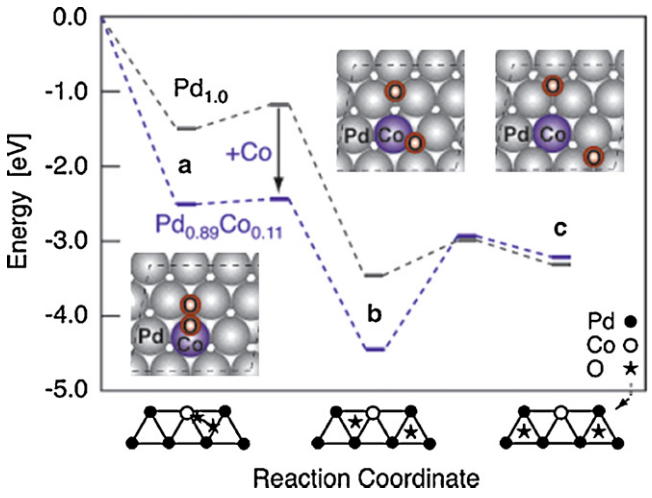

Fig. 15. Energy pathway for the dissociation of O_2 on Pd(1 1 1) (upper gray curve) and upon addition of 11% Co in the surface layer (lower blue curve) [95]. (For interpretation of the references to color in this figure legend, the reader is referred to the web version of the article.)

4. Durability of Pd based electrocatalysts

The thermodynamic behavior of bulk Pt is described by the Potential-pH diagrams (Pourbaix diagrams) [137]. The main pathways for Pt dissolution involve either the direct dissolution of metal,

$$Pt \rightarrow Pt^{2+} + 2e^-, \quad E_0 = 1.19 + 0.029\log[Pt^{2+}] \tag{4}$$

or an oxide film formation and a subsequent chemical reaction.

$$Pt + H_2O \rightarrow PtO + 2H^+ + 2e^-, \quad E_0 = 0.98 - 0.59pH \tag{5}$$

$$PtO + 2H^+ \rightarrow Pt^{2+} + H_2O, \quad \log(Pt^{2+}) = -7.06 - 2pH \tag{6}$$

The dissolution through Pt oxides is expected to be slow due to the self-passivation effect. Similar to Pt, Pd can dissolve in acid solution via [137]:

$$Pd \rightarrow Pd^{2+} + 2e^-, \quad E_0 = 0.99 + 0.029\log[Pd^{2+}] \tag{7}$$

or,

$$Pd + H_2O \rightarrow PdO + 2H^+ + 2e^-, \quad E_0 = 0.90 - 0.59pH \tag{8}$$

$$PdO + 2H^+ \rightarrow Pd^{2+} + H_2O, \quad \log(Pd^{2+}) = -2.35 - 2pH \tag{9}$$

In the direct dissolution pathway, the equilibrium potential of Pd dissolution is 0.2 V lower than that of Pt. In the chemical dissolution pathway, the Pd^{2+} equilibrium concentration is ~5 orders of magnitude higher than Pt^{2+}. Thus, Pd is much less stable than Pt in an acid medium [138]. One of the critical issues of low temperature fuel cells is the gradual loss of performance due to the degradation of the Pt-based catalyst layer under the harsh operating conditions including high temperature, high potential, low pH and frequent start–stop cycling [2,4]. Pd, which is much more easily dissolved, is not expected to meet the durability requirement of the PEMFC, especially for those in the automotive application due to intensive start–stop driving cycles. The very low stability of Pd/C during potential cycling was confirmed recently [139]. The stability of Pd in alkaline medium may not be a problem; however, no such study is available in the literature.

One way to improve the stability of Pd-based catalysts is to alloy with certain elements. Pd ternary alloys, including Pd–Co–Au [94,95] and Pd–Co–Mo [96], have been developed to improve the stability of the catalysts. The addition of 10% Au to the Pd–Mo mixture improved catalyst stability. However, the long-term durability of these catalysts has not been addressed yet. One interesting observation is that the PdCo and PdFe catalysts last longer in the acid-containing methanol under potential cycling [140]. The results may suggest that the Pd-based catalysts are more suitable for the direct alcohol fuel cells than for the hydrogen fuel cells as cathode materials.

Another promising way to improve the activity and durability of Pd alloys is to deposit a Pt layer on them. Recently, Pd/C and PdM/C catalysts modified by a Pt monolayer were found to possess higher activity than that of Pt/C due to the strain and electronic effects from the Pd-based cores, and the durability of the catalysts is improved significantly and comparable to Pt/C [115,139,141,142]. The Pd-based core materials are expected to be partially dissolved under the fuel cell operation conditions due to some pinholes in the Pt monolayer. In the meantime, the diffusion of Pt atoms on the surface results in a more compact shell. Thus, further dissolution of Pd-based core is greatly reduced. During the start–stop cycling of the fuel cell, the dissolved Pd cations diffuse and precipitate in the membrane forming a Pd band consisting of Pd nanoparticles. The effect of this Pd band on the performance of the fuel cell and stability of the membrane have not been understood.

5. Conclusions

Pd-based electrocatalysts may play a role to replace or partially replace costly Pt in both the anode and cathode of low temperature fuel cells. Pd–Pt alloys and other noble metal surfaces modified by Pd show comparable to or higher hydrogen oxidation activity than pure Pt either in pure hydrogen or CO containing fuel. The mechanisms of activity improvement for HOR and CO tolerance have not been fully understood. More experimental and theoretical studies are needed to understand the combination of structural and electronic effects on the fuel oxidation kinetics. The other aspect that needs to be addressed is the performance of Pd-based anode electrocatalysts in a fuel cell with very low noble metal loadings, for instance 0.05 mg cm^{-2}. So far, all the performances of Pd-based anode materials in a fuel cell were measured with a high noble metal loading resulting in a low utilization of the catalyst. Thus, the high activity of such catalysts is still questionable. In out of fuel cell testing, the higher HOR activity of such materials has not been fully confirmed either, due to difficulty of measuring kinetic current density. Kinetics studies of HOR using micro-electrode, gas diffusion electrode, and rotating disk electrode with ultralow catalyst loading are strongly encouraged. Finally, the structural stability of Pd-based electrocatalysts in an H_2 environment is also of interest to investigate.

Oxygen reduction rate seems to depend strongly on the orientations of the Pd surface with Pd(1 0 0) having a much higher ORR activity than any other facet in acid. Similarly, the (1 0 0) surfaces of Pd alloys are expected to exhibit high ORR activity. The single crystal studies of Pd and Pd alloys are very important to understand the facet dependence of oxygen reduction in both acid and alkaline solutions. Unfortunately, such studies are very rare. Synthesis and characterization of shape controlled Pd and Pd alloy nanomaterials are of importance to design next generation Pd-based electrocatalysts.

Generally, the particle size control and dispersion of Pd-based nanomaterials are more difficult than those of Pt-based ones. Systematic studies of the effects of synthesis methods, particle size, alloy degree, and composition on ORR activity and stability are crucial for optimization of Pd-based electrocatalysts. One should be very careful when comparing the activities of Pd-based nanomaterials reported in the literatures due to the difference in the compositions, particle sizes, synthesis methods, etc.

The long term durability of Pd-based electrocatalysts is one of the unavoidable issues for PEM fuel cell applications. Pd–Pt

based ORR catalysts are more stable than Pd-transition metal alloys under harsh fuel cell conditions, but may still not meet the long term fuel cell operation requirement due to the Pd leaching out. Future research may focus on improving the durability of Pd-based catalysts by surface modification and composition optimization. Core–shell type of catalyst with Pd-based materials as the core and Pt as the shell may be one of the most promising candidates to be used in the automotive fuel cell due to its low Pt content, high activity and stability. Future studies should focus on further enhancing the activity and durability by modifying the Pd-based core, and access the potential issues of leached Pd in the MEA during fuel cell operation.

References

[1] W. Vielstich, A. Lamm, H. Gasteiger, Handbook of Fuel Cells – Fundamentals, Technology and Applications, Wiley, West Sussex, 2003.
[2] K. Sasaki, M.H. Shao, R.R. Adzic, in: F.N. Buchi, M. Inaba, J. Schmidt (Eds.), Proton Exchange Membrane Fuel Cell Durability, Springer, New York, 2009, pp. 7–28.
[3] R.R. Adzic, J. Zhang, K. Sasaki, M.B. Vukmirovic, M. Shao, J.X. Wang, A.U. Nilekar, M. Mavrikakis, J.A. Valerio, F. Uribe, Top. Catal. 46 (2007) 249–262.
[4] H.A. Gasteiger, S.S. Kocha, B. Sompalli, F.T. Wagner, Appl. Catal. B: Environ. 56 (2005) 9–35.
[5] M. Lefevre, E. Proietti, F. Jaouen, J.P. Dodelet, Science 324 (2009) 71–74.
[6] www.monex.com.
[7] S.Q. Song, Y. Wang, P. Tsiakaras, P.K. Shen, Appl. Catal. B: Environ. 78 (2008) 381–387.
[8] E. Antolini, Energy Environ. Sci. 2 (2009) 915–931.
[9] C. Bianchini, P.K. Shen, Chem. Rev. 109 (2009) 4183–4206.
[10] M.W. Breiter, in: W. Vielstich, A. Lamm, H.A. Gasteiger (Eds.), Handbook of Fuel Cells, Wiley, 2003, pp. 361–367.
[11] N.M. Markovic, in: W. Vielstich, A. Lamm, H.A. Gasteiger (Eds.), Handbook of Fuel Cells, Wiley, New York, 2003, pp. 368–393.
[12] A. Chen, A. Kucernak, J. Phys. Chem. B 108 (2004) 13984.
[13] J.X. Wang, T.E. Springer, R.R. Adzic, J. Electrochem. Soc. 153 (2006) A1732.
[14] J.X. Wang, T.E. Springer, P. Liu, M. Shao, R.R. Adzic, J. Phys. Chem. C 111 (2007) 12425–12433.
[15] P.M. Quaino, J.L. Fernandez, M.R.G. de Chialvo, A.C. Chialvo, J. Mol. Catal. A: Chem. 252 (2006) 156–162.
[16] J. Tafel, Z. Phys. Chem. Stoechim. Verwandtschaftsl. 50 (1905) 641.
[17] J. Heyrovsky, Recl. Trav. Chim. Pays-Bas 46 (1927) 582.
[18] T. Volmer, M. Erdey-Gruz, Z. Phys. Chem. Abt. A 150 (1930) 203.
[19] C. Gabrielli, P.P. Grand, A. Lasia, H. Perrot, J. Electrochem. Soc. 151 (2004) A1937–A1942.
[20] P.N. Bartlett, B. Gollas, S. Guerin, J. Marwan, Phys. Chem. Chem. Phys. 4 (2002) 3835–3842.
[21] M.S. Rau, P.M. Quiano, M.R. Gennero de Chialvo, A.C. Chialvo, Electrochem. Commun. 10 (2008) 208–212.
[22] R. Parsons, Trans. Faraday Soc. 54 (1958) 1053.
[23] H. Gerischer, Z. Phys. Chem. N.F. 8 (1956) 137.
[24] L.I. Krishtalik, in: P. Delahay, C. Tobias (Eds.), Advances in Electrochemistry and Electrochemical Engineering, John Wiley & Sons, New York, 1970.
[25] S. Trasatti, J. Electroanal. Chem. 39 (1972) 163.
[26] J.K. Nørskov, T. Bligaard, A. Logadottir, J.R. Kitchin, J.G. Chen, S. Pandelov, J. Electrochem. Soc. 152 (2005) J23–J26.
[27] J.K. Nørskov, T. Bligaard, A. Logadottir, J.R. Kitchin, J.G. Chen, S. Pandelov, U. Stimming, J. Electrochem. Soc. 153 (2006) L33.
[28] N.M. Markovic, C.A. Lucas, V. Climent, V. Stamenkovic, P.N. Ross, Surf. Sci. 465 (2000) 103–114.
[29] J. Greeley, J.K. Norskov, L.A. Kibler, A.M. El-Aziz, D.M. Kolb, ChemPhysChem 7 (2006) 1032–1035.
[30] T.J. Schmidt, V. Stamenkovic, N.M. Markovic, P.N. Ross, Electrochim. Acta 48 (2003) 3823–3828.
[31] P. Liu, J.K. Norskov, Phys. Chem. Chem. Phys. 3 (2001) 3814.
[32] P.S. Ruvinsky, S.N. Pronkin, V.I. Zaikovskii, P. Bernhardt, E.R. Savinova, Phys. Chem. Chem. Phys. 10 (2008) 6665–6676.
[33] H.A. Gasteiger, J.E. Panels, S.G. Yan, J. Power Sources 127 (2004) 162–171.
[34] N.A. Maiorova, A.A. Mikhailova, O.A. Khazova, V.A. Grinberg, Russ. J. Electrochem. 42 (2006) 331–338.
[35] M.J. Escudero, E. Hontanon, S. Schwartz, M. Boutonnet, L. Daza, J. Power Sources 106 (2002) 206–214.
[36] S.A. Grigoriev, E.K. Lyutikova, S. Martemianov, V.N. Fateev, Int. J. Hydrogen Energy 32 (2007) 4438–4442.
[37] Y.H. Cho, B. Choi, Y.H. Cho, H.S. Park, Y.E. Sung, Electrochem. Commun. 9 (2007) 378–381.
[38] S.N. Pronkin, A. Bonnefont, P.S. Ruvinskiy, E.R. Savinova, Electrochim. Acta 55 (2010) 3312–3323.
[39] M.H. Shao, unpublished data.
[40] K.C. Neyerlin, W. Gu, J. Jorne, H.A. Gasteriger, J. Electrochem. Soc. 154 (2007) B631–B635.
[41] A.R. Kucernak, E. Toyoda, Electrochem. Commun. 10 (2008) 1728–1731.
[42] Y. Sun, J. Lu, L. Zhuang, Electrochim. Acta 55 (2010) 844–850.
[43] P. Stonehart, Int. J. Hydrogen Energy 9 (1984) 921–928.
[44] P. Stonehart, US Patent 4,407,906 (1983).
[45] F. Kadirgan, A.M. Kannan, T. Atilan, S. Beyhan, S.S. Ozenler, S. Suzer, A. Yörür, Int. J. Hydrogen Energy 34 (2009) 9450–9460.
[46] F. Alcaide, G. Álvarez, P.L. Cabot, O. Miguel, A. Querejeta, Int. J. Hydrogen Energy 35 (2010) 11634–11641.
[47] A.C. Garcia, V.A. Paganin, E.A. Ticianelli, Electrochim. Acta 53 (2008) 4309–4315.
[48] S.J. Yoo, H.Y. Park, T.Y. Jeon, I.S. Park, Y.H. Cho, Y.E. Sung, Angew. Chem. Int. Ed. 47 (2008) 9307–9310.
[49] J.H. Fishman, US Patent 3,510,355 (1970).
[50] R.D. Richman, US Patent 3,510,356 (1970).
[51] D.C. Papageorgopoulos, M. Keijzer, J.B.J. Veldhuis, F.A.D. Bruijn, J. Electrochem. Soc. 149 (2002) A1400–1404.
[52] T.J. Schmidt, Z. Jusys, H.A. Gasteiger, R.J. Behm, U. Endruschat, H. Boennemann, J. Electroanal. Chem. 501 (2001) 132–140.
[53] M.R. Tarasevich, V.A. Bogdanovskaya, B.M. Grafov, N.M. Zagudaeva, K.V. Rybalka, A.V. Kapustin, Y.A. Kolbanovskii, Russ. J. Electrochem. 41 (2005) 746–757.
[54] M.S. Chen, D.W. Goodman, Science 306 (2004) 252.
[55] M.T. Giacomini, M. Balasubramanian, S. Khalid, J. McBreen, E.A. Ticianellia, J. Electrochem. Soc. 150 (2003) A588–A593.
[56] A. Damjanovic, V. Brusic, Electrochim. Acta 12 (1967) 1171–1184.
[57] N.M. Markovic, R.R. Adzic, B.D. Cahan, E.B. Yeager, J. Electroanal. Chem. 377 (1994) 249–259.
[58] S. Kondo, M. Nakamura, N. Maki, N. Hoshi, J. Phys. Chem. C 113 (2009) 12625–12628.
[59] R.R. Adzic, in: J. Lipkowski, P.N. Ross (Eds.), Frontiers in Electrochemistry, Wiley-VCH, New York, 1998.
[60] M.H. Shao, P. Liu, R.R. Adzic, J. Am. Chem. Soc. 128 (2006) 7408–7409.
[61] M.R. Tarasevich, A. Sadkowski, E. Yeager, in: J.O.B.B.E. Conway, E. Yeager, S.U.M. Khan, R.E. White (Eds.), Comprehensive Treatise of Electrochemistry, Plenum Press, New York, 1983, p. 301.
[62] Y. Xu, A.V. Ruban, M. Mavrikakis, J. Am. Chem. Soc. 126 (2004) 4714.
[63] V. Stamenkovic, B.S. Mun, K.J.J. Mayrhofer, P.N. Ross, N.M. Markovic, J. Rossmeisl, J. Greeley, J.K. Nørskov, Angew. Chem. Int. Ed. 45 (2006) 2897–2901.
[64] J. Zhang, M.B. Vukmirovic, Y. Xu, M. Mavrikakis, R.R. Adzic, Angew. Chem. Int. Ed. 44 (2005) 2132–2135.
[65] Y. Xu, J. Greeley, M. Mavrikakis, J. Am. Chem. Soc. 127 (2005) 12823–12827.
[66] V.R. Stamenkovic, B. Fowler, B.S. Mun, G. Wang, P.N. Ross, C.A. Lucas, N.M. Markovic, Science 315 (2007) 493.
[67] J.K. Norskov, J. Rossmeisl, A. Logadottir, L. Lindqvist, J.R. Kitchin, T. Bligaard, H. Jonsson, J. Phys. Chem. B 108 (2004) 17886–17892.
[68] M.H. Shao, T. Huang, P. Liu, J. Zhang, K. Sasaki, M.B. Vukmirovic, R.R. Adzic, Langmuir 22 (2006) 10409–10415.
[69] V. Climent, N.M. Markovic, P.N. Ross, J. Phys. Chem. B 104 (2000) 3116–3120.
[70] M. Arenz, T.J. Schmidt, K. Wandelt, P.N. Ross, N.M. Markovic, J. Phys. Chem. B 107 (2003) 9813–9819.
[71] F.H.B. Lima, J. Zhang, M. Shao, K. Sasaki, B. Vukmirovic, E.A. Ticianelli, R.R. Adzic, J. Phys. Chem. C 111 (2007) 404–410.
[72] H. Naohara, S. Ye, K. Uosaki, Electrochim. Acta 45 (2000) 3305–3309.
[73] T.J. Schmidt, V. Stamenkovic, M. Arenz, N.M. Markovic, P.N. Ross, Electrochim. Acta 47 (2002) 3765–3776.
[74] Z. Dursun, Ş. Ulubay, B. Gelmez, F. Ertaş, Catal. Lett. 132 (2009) 127–132.
[75] V.M. Jalan, F.J. Luczak, J. Lee, US Patent 4,192,967 (1980).
[76] D.A. Landsman, F.J. Luczak, US Patent 4,316,944 (1982).
[77] D.A. Landsman, F.J. Luczak, in: W. Vielstich, A. Lamm, H.A. Gasteiger (Eds.), Handbook of Fuel Cells, Wiley, 2003, p. 811.
[78] V. Jalan, E.J. Taylor, J. Electrochem. Soc. 130 (1983) 2299.
[79] M.T. Paffett, J.G. Beery, S. Gottesfeld, J. Electrochem. Soc. 135 (1988) 1431.
[80] S. Mukerjee, S. Srinivasan, M. Soriaga, J. McBreen, J. Electrochem. Soc. 142 (1995) 1409.
[81] T. Toda, H. Igarashi, H. Uchida, M. Watanabe, J. Electrochem. Soc. 146 (1999) 3750.
[82] T. Toda, H. Igarashi, M. Watanabe, J. Electrochem. Soc. 145 (1998) 4185.
[83] U.A. Paulus, A. Wokaun, G.G. Scherer, T.J. Schmidt, V. Stamenkovic, N.M. Markovic, P.N. Ross, Electrochim. Acta 47 (2002) 3787–3798.
[84] U.A. Paulus, A. Wokaun, G.G. Scherer, T.J. Schmidt, V. Stamenkovic, V. Radmilovic, N.M. Markovic, P.N. Ross, J. Phys. Chem. B 106 (2002) 4181.
[85] B. Hammer, J.K. Nørskov, Surf. Sci. 343 (1995) 211.
[86] B. Hammer, J.K. Nørskov, Adv. Catal. 45 (2000) 71.
[87] J.R. Kitchin, J.K. Nørskov, M.A. Barteau, J.G. Chen, Phys. Rev. Lett. 93 (2004) 156801.
[88] J.R. Kitchin, J.K. Nørskov, M.A. Barteau, J.G. Chen, J. Chem. Phys. 120 (2004) 10240.
[89] J. Greeley, J.K. Nørskov, M. Mavrikakis, Annu. Rev. Phys. Chem. 53 (2002) 319–348.
[90] M.H. Shao, K. Sasaki, R.R. Adzic, J. Am. Chem. Soc. 128 (2006) 3526.
[91] D.B. Sepa, M.V. Vojnovic, L.M. Vracar, A. Damjanovic, Electrochim. Acta 32 (1987) 129–134.
[92] O. Savadogo, K. Lee, K. Oishi, S. Mitsushima, N. Kamiya, K.I. Ota, Electrochem. Commun. 6 (2004) 105–109.
[93] J.L. Fernandez, V. Raghuveer, A. Manthiram, A.J. Bard, J. Am. Chem. Soc. 127 (2005) 13100–13101.

[94] J.L. Fernandez, D.A. Walsh, A.J. Bard, J. Am. Chem. Soc. 127 (2005) 357–365.
[95] J.L. Fernandez, J.M. White, Y.M. Sun, W.J. Tang, G. Henkelman, A.J. Bard, Langmuir 22 (2006) 10426–10431.
[96] V. Raghuveer, A. Manthiram, A.J. Bard, J. Phys. Chem. B 109 (2005) 22909–22912.
[97] J. Mathiyarasuz, K.L.N. Phani, J. Electrochem. Soc. 154 (2007) B1100–B1105.
[98] W. Wang, D. Zheng, C. Du, Z. Zou, X. Zhang, B. Xia, H. Yang, D.L. Akins, J. Power Sources 167 (2007) 243–249.
[99] L. Zhang, K. Lee, J.J. Zhang, Electrochim. Acta 52 (2007) 3088–3094.
[100] R.F. Wang, S.J. Liao, Z.Y. Fu, S. Ji, Electrochem. Commun. 10 (2008) 523–526.
[101] M.R. Tarasevich, G.V. Zhutaeva, V.A. Bogdanovskaya, M.V. Radina, M.R. Ehrenburg, A.E. Chalykh, Electrochim. Acta 52 (2007) 5108–5118.
[102] Y. Xu, M.H. Shao, M. Mavrikakis, R.R. Adzic, in: M.T.M. Koper (Ed.), Fuel Cell Catalysis: A Surface Science Approach, John Wiley & Sons, 2009, pp. 271–316.
[103] A. Sarkar, A.V. Murugan, A. Manthiram, J. Mater. Chem. 19 (2009) 159–165.
[104] A.A. Serov, S.-Y. Cho, S. Han, M. Min, G. Chai, K.H. Nam, C. Kwak, Electrochem. Commun. 9 (2007) 2041–2044.
[105] L. Cheng, Z. Zhang, W. Niu, G. Xu, L. Zhu, J. Power Sources 182 (2008) 91–94.
[106] H. Li, G. Sun, N. Li, S. Sun, D. Su, Q. Xin, J. Phys. Chem. C 111 (2007) 5605–5617.
[107] S. Guerin, B.E. Hayden, C.E. Lee, C. Mormiche, A.E. Russell, J. Phys. Chem. B 110 (2006) 14355–14362.
[108] H.C. Ye, R.M. Crooks, J. Am. Chem. Soc. 129 (2007) 3627–3633.
[109] X.P. Wang, N. Kariuki, J.T. Vaughey, J. Goodpaster, R. Kumar, D.J. Myers, J. Electrochem. Soc. 155 (2008) B602–B609.
[110] D.J. Myers, DOE Hydrogen and Fuel Cell Review Meeting, Arlington, VA, 2008.
[111] V. Raghuveer, P.J. Ferreira, A. Manthiram, Electrochem. Commun. 8 (2006) 807–814.
[112] H. Liu, A. Manthiram, Electrochem. Commun. 10 (2008) 740–744.
[113] L. Xiao, L. Zhuang, Y. Liu, J. Lu, H.D. Abruna, J. Am. Chem. Soc. 131 (2008) 602–608.
[114] W.Z. Li, P. Haldar, Electrochem. Commun. 11 (2009) 1195–1198.
[115] M. Shao, K. Sasaki, P. Liu, R.R. Adzic, Z. Phys. Chem. 221 (2007) 1175–1190.
[116] L. Jiang, A. Hsu, D. Chu, R. Chen, J. Electrochem. Soc. 156 (2009) B643–B649.
[117] J. Kim, J.E. Park, T. Momma, T. Osaka, Electrochim. Acta 54 (2009) 3412–3418.
[118] B. Li, J. Prakash, Electrochem. Commun. 11 (2009) 1162–1165.
[119] M. Nie, P.K. Shen, Z.D. Wei, J. Power Sources 167 (2007) 69–73.
[120] S. Lu, J. Pan, A. Huang, L. Zhuang, J. Lu, Proc. Natl. Acad. Sci. U.S.A. 105 (2008) 20611–20614.
[121] S. Catanorchi, M. Piana, H.A. Gasteiger, ECS Trans. 16 (2008) 2045–2055.
[122] W.E. Mustain, K. Kepler, J. Prakash, Electrochim. Acta 52 (2007) 2102–2108.
[123] H.Q. Li, Q. Xin, W.Z. Li, Z.H. Zhou, L.H. Jiang, S.H. Yang, G.Q. Sun, Chem. Commun. (2004) 2776–2777.
[124] T. Lopes, E. Antolini, E.R. Gonzalez, Int. J. Hydrogen Energy 33 (2008) 5563–5570.
[125] K. Lee, O. Savadogo, A. Ishihara, S. Mitsushima, N. Kamiya, K. Ota, J. Electrochem. Soc. 153 (2006) A20–A24.
[126] W.E. Mustain, K. Kepler, J. Prakash, Electrochem. Commun. 8 (2006) 406–410.
[127] M. Tarasevich, V. Bogdanovskaya, L. Kuznetsova, A. Modestov, B. Efremov, A. Chalykh, Y. Chirkov, N. Kapustina, M. Ehrenburg, J. Appl. Electrochem. 37 (2007) 1503–1513.
[128] J.L. Rousset, J.C. Bertolini, P. Miegge, Phys. Rev. B 53 (1996) 4947.
[129] A.V. Ruban, H.L. Skriver, J.K. Nørskov, Phys. Rev. B 59 (1999) 15990.
[130] G. Bozzolo, R.D. Noebe, J. Khalil, J. Morse, Appl. Surf. Sci. 219 (2003) 149–157.
[131] Y.G. Suo, L. Zhuang, J.T. Lu, Angew. Chem. Int. Ed. 46 (2007) 2862–2864.
[132] M. Shao, P. Liu, J. Zhang, R.R. Adzic, J. Phys. Chem. B 111 (2007) 6772–6775.
[133] W.-P. Zhou, X. Yang, M.B. Vukmirovic, B.E. Koel, J. Jiao, G. Peng, M. Mavrikakis, R.R. Adzic, J. Am. Chem. Soc. 131 (2009) 12755–12762.
[134] V.R. Stamenkovic, B.S. Mun, K.J.J. Mayrhofer, P.N. Ross, N.M. Markovic, J. Am. Chem. Soc. 128 (2006) 8813–8819.
[135] Y.X. Wang, P.B. Balbuena, J. Phys. Chem. B 109 (2005) 18902–18906.
[136] F. Fouda-Onana, S. Bah, O. Savadogo, J. Electroanal. Chem. 636 (2009) 1–9.
[137] M. Pourbaix, Atlas of Electrochemical Equilibria, second ed., NACE, Houston, 1974.
[138] J. Solla-Gullón, V. Montiel, A. Aldaz, J. Clavilier, Electrochem. Commun. 4 (2002) 716–721.
[139] P.P. Wells, E.M. Crabb, C.R. King, R. Wiltshire, B. Billsborrow, D. Thompsett, A.E. Russell, Phys. Chem. Chem. Phys. 11 (2009) 5773–5781.
[140] M.H. Shao, R.R. Adzic, unpublished data.
[141] J. Zhang, M.B. Vukmirovic, K. Sasaki, F. Uribe, R.R. Adzic, J. Serb. Chem. Soc. 70 (2005) 513–525.
[142] M.H. Shao, K. Shoemaker, A. Peles, K. Kaneko, L. Protsailo, J. Am. Chem. Soc. 132 (2010) 9253–9255.